Ocean Engineering 149 (2018) 373–382

Contents lists available at ScienceDirect

Ocean Engineering

journal homepage: www.elsevier.com/locate/oceaneng

Controlling tracking trajectory of a robotic vehicle for inspection of underwater structures

Cristiano Zacarrias Ferreira, Reginaldo Cardoso *, Magno Enrique Mendoza Meza, Juan Pablo Julca Ávila

Graduate Program in Mechanical Engineering, Federal University of ABC (UFABC), Santo André SP09210-580, São Paulo, Brazil

ARTICLE INFO

Keywords:
Underactuated control
MIMO nonlinear control
Backstepping
Control Lyapunov Function (CLF)
Remotely Operated Vehicle (ROV)

ABSTRACT

This work presents nonlinear, multivariable control strategies, based on backstepping methodology and Control Lyapunov Function (CLF) for trajectory tracking problem of a Hybrid Remotely Operated Vehicle (HROV), which is under development at the Federal University of ABC (UFABC) since 2012. The main objective of the vehicle is to inspect underwater structures by measuring plates thickness. The design control for underactuated HROV presents some limitations in the vehicle trajectory. The control consists on the combination of two methodologies, which are the backstepping and the CLF. It also makes robustness study of controllers consider disturbance acting on the vehicle. The proposed control responded appropriately to the trajectories selected as reference and presents robustness for non-modeled external disturbances.

1. Introduction

There are applications of Remotely Operated Vehicles (ROV's) in a variety of areas, such as: biology, for marine habitat monitoring; archeology, for flooded site investigation and engineering, for submerged structures inspection and underwater mining.

The vehicle was named HROV (Hybrid Remotely Operated Vehicle) and the term hybrid installed due to its locomotion feature, which can use thrusters for a navigation on the water or a pair of motorized tracks for movement over the structure.

The Brazilian navy regulates that the release for operation of vessels has to be in national waters. This must be made through a complete dry deck inspection, in addition to a technical assessment of the thickness plates in the case of metallic vessels with more than fifteen years of operation (DPC, 2013). 超过15年的船必须进行干式甲板检测

Among the Naval applications, we can highlight a niche in the petroleum area that, in addition to using large ships in transportation, have Floating Production, Storing and Offloading (FPSO) structures for the production and storage in the offshore oil and oil products. These structures are designed to work in the same lease for up to 25 years and the withdrawal of a vessel in operation influences financial loss (Whitcomb, 2000). The inspection of the structure in place is necessary for this type of application.

In this scenario, 方案 in the Federal University of ABC (UFABC), we developed a project with the objective of developing a HROV (named Proteo) for inspection of underwater metallic structures in their normal operating environment, performing plate thickness measurements by ultrasonic sensor.

The project considers a control station, which is nearby the structure to be inspected or in a location, that allows the remote activation of the HROV with the umbilical communication. The vehicle is placed in the water and positioned by the operator using the thrusters. At the initial point of inspection, the HROV performs a rotation maneuver to keep the motorized tracks in contact with the structure and to do this is necessary that the vertical thrusters maintain a normal force to the inspection plane, causing the motorized tracks to have sufficient friction to maneuver the vehicle by performing the thickness measurements.

For the trajectory tracking problem, several control techniques are being used. In order to control an actuated ROV, in Srisamosorn et al. (2013)) was developed a robust adaptive control algorithm and used two Lyapunov candidate function to demonstrate the stability and to determine adaptive laws. The performance is verified with numerical simulation; in Encarnacao and Pascoal (2000) it was proposed a methodology utilizing a nonlinear dynamic inversion and applying backstepping techniques; in Zhu and Gu (2011a) it was proposed a combining of two controllers: an adaptive backstepping technique and a sliding control; in

* Corresponding author.
E-mail addresses: cristianozf@hotmail.com (C.Z. Ferreira), reginaldo.cardoso@ufabc.edu.br (R. Cardoso), magno.meza@ufabc.edu.br (M.E.M. Meza), juan.avila@ufabc.edu.br (J.P.J. Ávila).

https://doi.org/10.1016/j.oceaneng.2017.12.032
Received 19 July 2017; Received in revised form 8 November 2017; Accepted 10 December 2017
Available online 27 December 2017

Patompak and Nilkhamhang (2012) it was developed an adaptive backstepping sliding-mode controller; in Fernandes et al. (2015) it was proposed a motion control system, which is an output feedback control composed of a MIMO PID controller, feedforward and high-gain observer.

For the control of an underactuated ROV, in Raygosa-Barahona et al. (2011) it was applied a combining of two controllers, a backstepping and a second order integral sliding modes controls; in Do (2010) it was proposed a control design based on several nonlinear coordinate changes, the transverse function approach the backstepping technique, the Lyapunov direct method and utilization of the ship dynamics; in Khadhraoui et al. (2014) it was developed the design control on the vertical plane with a backstepping methodology.

This article aims to give the next step of the project, which is the development of a navigation control for this HROV, which is underactuated, i.e., the direction sway, y, is not actuated, because of this it was necessary to combine two control techniques. The idea is to divide the vehicle model into two parts: the first part is considered fully actuated and is controlled with a backstepping control, this part of movement is provided by the four thrusters positioned in the vertical. The second part where the underactuated occurs, the movement is provided by two thrusters positioned in the horizontal.

In order to control the sub actuated part, it was used the ideas proposed in Fierro and Lewis (1995); Zidani et al. (2015), in which were developed a kinematic/torque control law for a wheeled mobile robot utilizing backstepping. The control Lyapunov function was used due to the need for a bottleneck, thus the underactuated model is very similar of a ship model (Liu et al., 2016; Jiang, 2002; Do, 2010).

The paper is organized as follows: Section 2, introduces the Proteo architecture; Section 3, shows the vehicle mathematical model; Section 4, presents the control design; Section 5, concerns the numerical simulation and Section 6, conclusions.

2. Proteo hardware architecture

The main function of the vehicle is the inspection of ship hulls by means of ultrasonic transducers to check the thickness of the plate and look for cracks.

It has two operating modes: free flight and crawling. In the first mode of operation, the vehicle uses six thrusters (4 vertical and 2 horizontal) for its displacement through the water and in the second mode, uses two motorized mats for its locomotion on the surface of the hull of the ship and 4 vertical thrusters to apply a normal force in the hull, avoiding the use of complex electromagnetic devices.

2.1. Mechanical designed

The structure of HROV consists in a polypropylene plates and its divided in 5 parts, two lateral and three horizontal plates. The top horizontal plate of the structure contains the float and four thrusters with their Vertically oriented axes; the middle plate contains a pressure vessel for the control of the electronics and the lower part of the structure contains two thrusters with their axes oriented horizontally as motorized tracks. In the initial design the float should be a block (Fig. 1), but due to the weight of the motorized tracks, tubes were used (Fig. 2).

An umbilical cable is used for an electrical signal and a signal transmission, which can be seen in Figs. 2 and 1.

It is noted that the general structure can be approximated being symmetrical in the longitudinal and transverse planes, which will influence the simplifications that will be made in the mathematical modeling, section 3.

2.2. Computer, sensors and actuators

Tiger board is a high performance computer manufactured by Versalogic Corporation that supports other PC/104 and PC/104-Plus expansion cards, and features an Intel Atom Z5xx processor. Tiger is compatible with Windows, Windows Embedded, Linux, VxWorks and QNX. In this work we used the Debian 6.0.0 operating system (Squeeze/Stable) (Versa Logic Corporation). The Fig. 3 shows schematically the architecture adopted for the project. It has a surface computer from which the vehicle is remotely controlled and an embedded, where the program that processes the data of the sensors, receives the desired trajectory and locally controls the actuators to keep the vehicle in the trajectory.

Sensors used in the HROV were chosen to provide information capable of giving orientation, position, speed and acceleration of the vehicle. The altimeter model PA500/6-PS (manufactured by Tritech International Limited) provides underwater distance measurements. In this design, the sensor is used to measure the distance between the vehicle and the inspected surface (Tritech International Ltd).

Velocity Log Doppler sensor (NavQuest 600 manufactured by LinkQuest Inc.) provides the speed of the vehicle in the surge, sway and pitch directions (LinkQuest Inc).

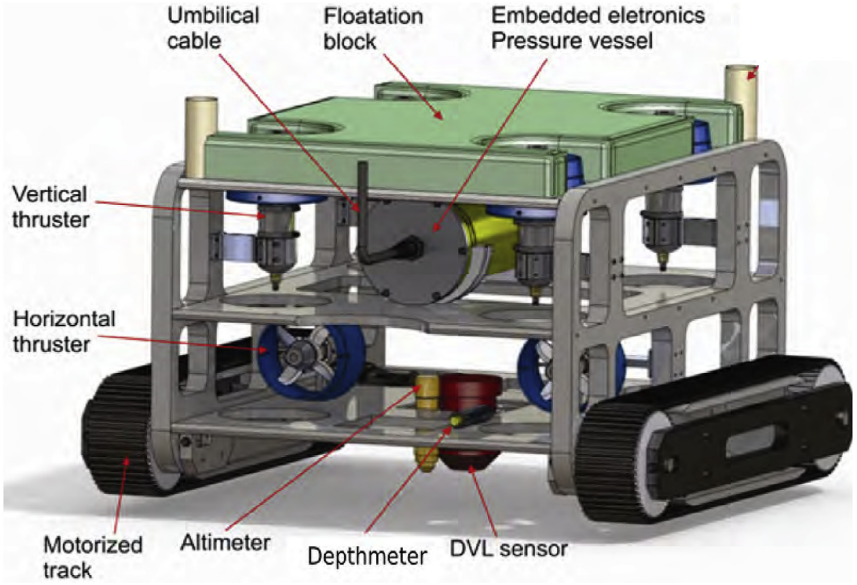

Fig. 1. The design of the HROV Proteo (Luque and Avila, 2013).

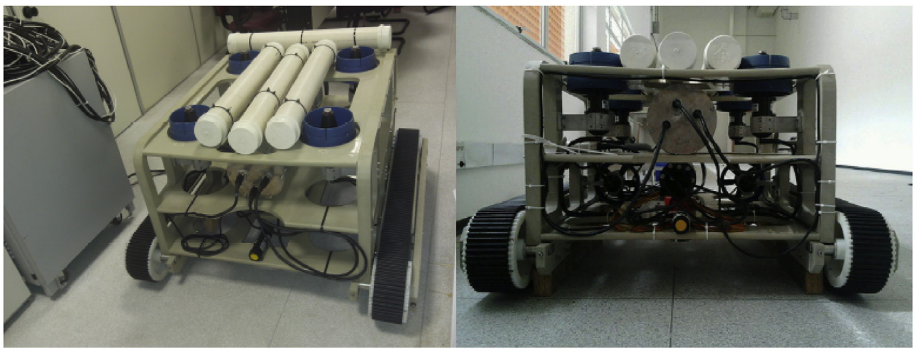

Fig. 2. The HROV Proteo. Designed and build at UFABC.

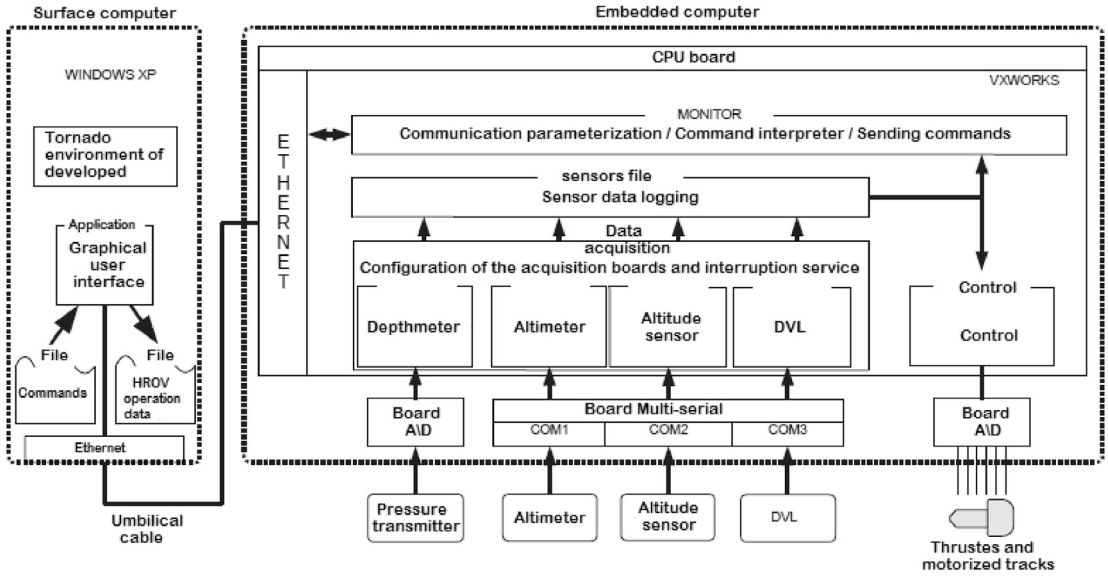

Fig. 3. Diagram of the control architecture.

The depth meter model TW-PI (manufactured by IOPE Ltd.) provides the vehicle depth, is the only analog sensor.

The embedded sensors are listed in Table 1. Proteo has 8 actuators for locomotion (manufactured by Tecnadyne Inc.), six thrusters model 1020 and two motors model 40. All of them are controlled by a power controller called ISOMOD (from the same manufacturer), which receives by a serial input the commands indicating the level of voltage to be placed at the output of each actuator. The main supply of the actuators is 150 V dc. For the activation of the board and sensors, other sources have been installed, whose function is to reduce the voltage level to 24 Vdc, 12 Vdc or 5 Vdc depending on the devices (Tecnadyne, 2040; Tecnadyne, 1020).

At Ferreira et al. (2014a) the curve of thrust by voltage about the thrusters was plotted and then it arrives in Equation (1)

$$F = aV^2 + bV + c \tag{1}$$

with $a = 11.97\ \mathrm{N/V^2}$, $b = -13.4388\ \mathrm{N/V}$ and $c = 5.1661\ \mathrm{N}$ to positive propulsion and $a = 7.2131\ \mathrm{N/V^2}$, $b = -8.5807\ \mathrm{N/V}$ and $c = 3.2986\ \mathrm{N}$ to negative propulsion.

3. Mathematical model of the dynamic

The mathematical model has 6 degrees of freedom (DOF), 3 about position (surge, sway and heave) and 3 about the orientation (roll, pitch, yaw) and two coordinates system (Ferreira et al., 2013). The body-fixed frame (X_B, Y_B and Z_B) is coincident with the vehicle center of gravity. The Earth-fixed frame (X_{EF}, Y_{EF} and Z_{EF}) is located out of the vehicle, as shown in Fig. 4. According to Zhu et al. (2012) the HROV equation can be expressed as Equation (2),

$$\dot{\boldsymbol{\eta}} = \boldsymbol{J}(\boldsymbol{\eta})\boldsymbol{\nu} \tag{2}$$

Table 1
HROV navigation sensors.

Variable	Sensor	Accuracy, sampling rate	Output
Distance to obstacle	Altimeter	±1 mm/s, 10 Hz	Digital
Linear velocities and altitude	Doppler Velocity Log	±1 mm/s, 3 Hz	Digital
Linear velocities	Altitude sensor	Orientation: 2%, 0.02°	Digital
Angular velocities		±0.3°/s	
Linear acceleration		1%	
Roll, Yaw and Pitch angles		71.1 Hz	
Depth	Depth meter	5 mm	Analog

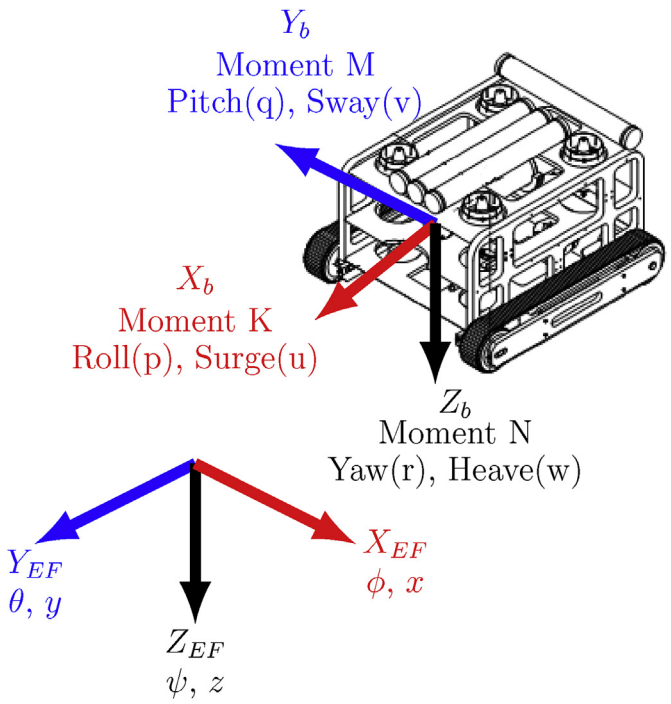

Fig. 4. Degrees of freedom of the Proteo HROV.

where $\boldsymbol{J}(\boldsymbol{\eta})$ is the Jacobian matrix of the system transformation,

$$\boldsymbol{J}(\boldsymbol{\eta}) = \begin{bmatrix} \boldsymbol{J}_1 & 0 \\ 0 & \boldsymbol{J}_2 \end{bmatrix}, \tag{3}$$

where,

$$\boldsymbol{J}_1 = \begin{bmatrix} c\psi c\theta & -s\psi c\phi + c\psi s\theta s\phi & s\psi s\phi + c\psi c\phi s\theta \\ s\psi c\theta & c\psi s\phi + s\psi s\theta s\phi & -c\psi s\phi + s\theta s\psi c\phi \\ -s\theta & c\theta s\phi & c\theta c\phi \end{bmatrix} \tag{4}$$

and

$$\boldsymbol{J}_2 = \begin{bmatrix} 1 & s\phi t\theta & c\phi t\theta \\ 0 & c\phi & -s\phi \\ 0 & s\phi/c\theta & c\phi/s\theta \end{bmatrix}, \tag{5}$$

wich $\nu = [u, v, w, p, q, r]^T$ is the linear and the angular velocity in the body-fixed frame, $\eta = [x, y, z, \phi, \theta, \psi]^T$ which is the position and Euler angles in the Earth-fixed frame, as shown in Fig. 4, $sx = \sin(x)$, $cx = \cos(x)$, and $tx = \tan(x)$. Assuming that the pitch and roll angles (θ and ϕ, respectively) are limited between $-\pi/2$ and $\pi/2$ (Zhu et al., 2012; Fossen, 1994).

$$\boldsymbol{M}\dot{\boldsymbol{\nu}} + \boldsymbol{C}(\boldsymbol{\nu})\boldsymbol{\nu} + \boldsymbol{D}(\boldsymbol{\nu})\boldsymbol{\nu} + \boldsymbol{g}(\boldsymbol{\eta}) = \boldsymbol{\tau}, \tag{6}$$

where the matrix $\boldsymbol{M}$ represents the sum of the rigid-body inertia and the inertia matrix; $\boldsymbol{C}(\boldsymbol{\nu})$ the sum of rigid-body Coriolis and the centripetal matrix with the mass; $\boldsymbol{D}(\boldsymbol{\nu})$ the hydrodynamic damping; $\boldsymbol{g}(\boldsymbol{\eta})$ force vector and gravitational moment and buoyancy; $\boldsymbol{\tau}$ the control force and the moment vector.

The dynamic equation of the HROV are Equations (2) and (6)

$$\begin{aligned} \boldsymbol{\tau} &= \boldsymbol{M}\dot{\boldsymbol{\nu}} + (\boldsymbol{C}(\boldsymbol{\nu}) + \boldsymbol{D}(\boldsymbol{\nu}))\boldsymbol{\nu} + \boldsymbol{g}(\boldsymbol{\eta}) \\ \dot{\boldsymbol{\eta}} &= \boldsymbol{J}(\boldsymbol{\eta})\boldsymbol{\nu} \end{aligned} \tag{7}$$

with

$$\boldsymbol{g}(\boldsymbol{\eta}) = \begin{bmatrix} \sin(\theta)(mg - \rho_A g) \\ -\cos(\theta)\sin(\phi)(mg - \rho_A g) \\ -\cos(\phi)\cos(\theta)(mg - \rho_A g) \\ -\rho_A g(zb\cos(\theta)\sin(\phi)) \\ -\rho_A g(zb\sin(\theta)) \\ 0 \end{bmatrix},$$

$$\boldsymbol{M} = diag\begin{bmatrix} m - X_{\dot{u}}, & m - Y_{\dot{v}}, & m - Z_{\dot{w}} \dots \\ \dots I_x - K_{\dot{p}}, & I_y - M_{\dot{q}}, & I_z - N_{\dot{r}} \end{bmatrix},$$

$$\boldsymbol{D}(\boldsymbol{\nu}) = diag\begin{bmatrix} X_u + X_{u|u|}u, & Y_v + Y_{v|v|}v, & Z_w + Z_{w|w|}w \\ K_p + K_{p|p|}p, & M_q + M_{q|q|}q, & N_r + N_{r|r|}r \end{bmatrix},$$

$$\boldsymbol{C}(\boldsymbol{\nu}) = \begin{bmatrix} 0 & 0 & 0 \\ 0 & 0 & 0 \\ 0 & 0 & 0 \\ 0 & (m - Z_{\dot{w}})w & -(m - Y_{\dot{v}})v \\ -(m - Z_{\dot{w}})w & 0 & (m - X_{\dot{u}})u \\ (m - Y_{\dot{v}})v & -(m - X_{\dot{u}})u & 0 \\ 0 & (m - Z_{\dot{w}})w & -(m - Y_{\dot{v}})v \\ -(m - Z_{\dot{w}})w & 0 & (m - X_{\dot{u}})u \\ (m - Y_{\dot{v}})v & -(m - X_{\dot{u}})u & 0 \\ 0 & (I_z - N_{\dot{r}})r & -(I_y - M_{\dot{q}})q \\ (I_z - N_{\dot{r}})r & 0 & (I_x - K_{\dot{p}})p \\ (I_y - M_{\dot{q}})q & -(I_x - K_{\dot{p}})p & 0 \end{bmatrix},$$

$$\boldsymbol{\tau} = [X\ 0\ Z\ K\ M\ N]^T.$$

For the identification of the HROV parameters, tests were carried out in the test tank, being reported in the work (Ferreira et al., 2014b).

4. Control design

For the under actuated system, the plant was divided in two parts, one controlled for the movement in the XY plane and another for the other degrees of freedom. The diagram of the controllers can be seen in Fig. 5. The control in the plane was divided in two stages: kinematic and dynamic controller. We chose the control Lyapunov function (CLF) associated with backstepping.

4.1. Control Lyapunov function

The equations of motion that will be adopted for the *XY* plane were

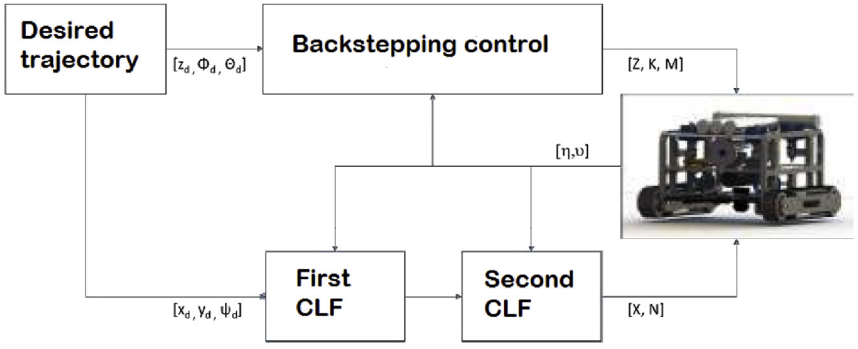

Fig. 5. Architecture of the Proteo controllers.

obtained from Equation (7) considering that the HROV is maintained in the XY plane with $\phi = 0$ and $\theta = 0$, that way, the position and velocity vectors are: $\nu = [u, v, r]^T$ and $\eta = [x, y, \psi]^T$ the system of XY plane is:

$$\begin{aligned}
&\dot{x} = u\cos(\psi) - \sin(\psi)\\
&\dot{y} = u\sin(\psi) + v\cos(\psi)\\
&\dot{\psi} = r\\
&\dot{u} = \frac{1}{m - X_{\dot{u}}}\Big[(m - Y_{\dot{v}})vr - \big(X_u + X_{u|u|}|u|\big)u - \ldots\\
&\ldots - (m - Z_{\dot{w}})wq + X\Big]\\
&\dot{v} = \frac{1}{m - Y_{\dot{v}}}\Big[- (m - X_{\dot{u}})ur - \big(Y_v + Y_{v|v|}|v|\big)v - \ldots\\
&\ldots - (- m + Z_{\dot{w}})wp\Big]\\
&\dot{r} = \frac{1}{I_z - N_{\dot{r}}}\Big[- (X_{\dot{u}} - Y_{\dot{v}})uv - \big(N_r + N_{r|r|}|r|\big)r + \ldots\\
&\ldots + \big(I_x - I_y - K_{\dot{p}} + M_{\dot{q}}\big)pq + N\Big]
\end{aligned}$$

As previously mentioned, the HROV equations of motion were separated to treat the problem of under actuated. The same approach is used in vehicles with differential wheels. For this purpose the development of this controller is based on the control proposals adopted by Fierro and Lewis (1995); Zidani et al. (2015). Basically the idea of the controller is to propose the tracking of the desired trajectory. The problem is to converge to zero the position errors in a given instant.

Considering the under actuated of the vehicle, the trajectories that it performs are not arbitrary, it has some restrictions, as indicated by Do and Pan (2009)

- The desired velocity u_d and r_d satisfy:

$$\begin{aligned}
&u_d = \sqrt{\dot{x}_d^2 + \dot{y}_d^2}\\
&r_d = \frac{\dot{x}_d\ddot{y}_d - \dot{y}_d\ddot{x}_d}{\dot{x}_d^2 + \dot{y}_d^2}
\end{aligned} \tag{8}$$

- The desired trajectory has to be a continuous function. If the intention is to perform a trajectory that is not regular, it becomes necessary to separate the trajectories in regular parts;
- The desired velocity should not be zero, it is not a control to stabilize the vehicle at one point, but rather to track a desired trajectory. Another imposed condition is that the vehicle acceleration is limited and the velocity variations are slowly, which is reasonable considering the inertia of the vehicle in the water.
- The surge velocity is always higher than a possible sway velocity, which is justifiable because the vehicle is under actuated. In a practical application the most common trajectories for the vehicle are met, such as straight, curved and sinusoidal lines, always having the surge direction as the direction of the trajectory;

The problem becomes to converge to zero the position errors between the HROV and the desired trajectory. The definition of the trajectory error,

$$\begin{bmatrix} e_1\\ e_2\\ e_3 \end{bmatrix} = \begin{bmatrix} \cos(\psi) & \sin(\psi) & 0\\ \sin(\psi) & \cos(\psi) & 0\\ 0 & 0 & 1 \end{bmatrix}\begin{bmatrix} x_d - x\\ y_d - y\\ \psi_d - \psi \end{bmatrix} \tag{9}$$

We will replace the notation u by u_1 and r by r_1 to be easily understood.

It is observed that the trajectory tracking condition is: $(e_1, e_2, e_3) = (0, 0, 0)$. Where $x = x_d$, $y = y_d$ and $\psi = \psi_d$ and therefore $u_1 = u_d$, $v = v_d = 0$ and $r_1 = r_d$. The under actuated of the HROV doesn't allow the direct control of the heave velocity. According to Do (2010) an angular deviation (δ) is necessary to create a component of the surge velocity in the sway direction, the derivative of Equation (9) with δ

$$\begin{aligned}
e_{3\delta} &= e_3 + \delta\\
\dot{e}_1 &= -u_1 + re_2 + u_d\cos(e_{3\delta})\\
\dot{e}_2 &= -re_1 + u_d\sin(e_{3\delta})\\
\dot{e}_3 &= r_d - r_1
\end{aligned} \tag{10}$$

with $\left|\delta\right| < \frac{\pi}{4}$.

The function candidate to CLF was used in Fierro and Lewis (1995); Zidani et al. (2015)

$$V = \frac{1}{2}\left(e_1^2 + e_2^2\right) + \frac{1 - \cos(e_{3\delta})}{K_b} \tag{11}$$

where K_b is a positive constant. Differentiating Equation (11)

$$\dot{V} = (- u_1 + u_d\cos(e_3))e_1 + \left(u_d e_2 + \frac{r_d}{K_b} - \frac{r_1}{K_b}\right)\sin(e_3) \tag{12}$$

considering u_1 and r_1 the output of this controller (CLF), these variables were chosen to make sure that Equation (12) will be negative defined,

$$\begin{bmatrix} u_1\\ r_1 \end{bmatrix} = \begin{bmatrix} u_d\cos(e_{3\delta}) + K_a e_1\\ r_d + K_b u_d e_2 + K_c\sin(e_{3\delta}) \end{bmatrix} \tag{13}$$

$$\dot{V} = -K_a e_1^2 - \frac{K_c}{K_b}\sin(3_{3\delta})^2 \tag{14}$$

where K_a and K_c are positive real constants.

Although the intention to make the control outputs make Equation (12) negative defined, it is negative semidefinite, since it can present null values for entries other than zero, considering only integer multiples of π. The controller does not guarantee the asymptotic global stability of the vehicle, being able to have oscillations around the desired equilibrium point, however, as will be shown later in the simulations, the oscillations are not significant, which guarantees a good performance to the control.

Before starting the design of the dynamic controller, it is necessary to create two new variables,

$$\begin{aligned}
z_1 &= u_1 - u\\
z_2 &= r_1 - r
\end{aligned} \tag{15}$$

with this new variables, it was chosen two new Lyapunov function candidates,

$$\begin{aligned}
V_1 &= \frac{1}{2}z_1^2\\
\dot{V}_1 &= z_1(\dot{u}_1 - u)
\end{aligned} \tag{16}$$

$$\begin{aligned}
V_2 &= \frac{1}{2}z_2^2\\
\dot{V}_2 &= z_2(\dot{r}_1 - r).
\end{aligned} \tag{17}$$

To become Equations (16) and (17) negative defined, it was chosen X and N like the control variables

$$\begin{aligned}
X &= \big(X_u + X_{u|u|}|u|\big)u + (- m + Y_{\dot{v}})vr + \ldots\\
&\ldots + (m - Z_{\dot{w}})wq + (m - X_{\dot{u}})(\dot{u}_c + K_D z_1)\\
N &= \big(N_r + N_{r|r|}|r|\big)r + (X_{\dot{u}} - Y_{\dot{v}})uv + \ldots\\
&\ldots + \big(I_y - M_{\dot{q}} - I_x + K_{\dot{p}}\big)pq + \ldots\\
&\ldots + (I_z - N_{\dot{r}})(\dot{r}_c + K_E z_2)
\end{aligned} \tag{18}$$

with K_D and K_E are positive real constants.

4.2. Control backstepping

The next step is to control the others HROV degrees of freedom

(z, θ, ϕ). The reduced system is:

$$\begin{aligned} \boldsymbol{\tau}_z &= \boldsymbol{M}_z\dot{\boldsymbol{\nu}_z} + (\boldsymbol{C}_z(\boldsymbol{\nu}_z) + \boldsymbol{D}_z(\boldsymbol{\nu}_z))\boldsymbol{\nu}_z + \boldsymbol{g}_z(\boldsymbol{\eta}_z) \\ \dot{\boldsymbol{\eta}}_z &= \boldsymbol{J}_z(\boldsymbol{\eta}_z)\boldsymbol{\nu}_z \end{aligned} \tag{19}$$

where:

$$\begin{gathered} \boldsymbol{M}_z = diag\left[m - Z_{\dot{w}}, \quad I_x - K_{\dot{p}}, \quad I_y - M_{\dot{q}}\right], \\ \boldsymbol{C}_z(\boldsymbol{\nu}_z) + \boldsymbol{D}_z(\boldsymbol{\nu}_z) = \ldots \\ \ldots = \begin{bmatrix} Z_w + Z_{w|w|}|w| & (m - Y_{\dot{v}})v & (-m + X_{\dot{u}})u \\ (-m + Y_{\dot{v}})v & K_p + K_{p|p|}|p| & (I_z - N_{\dot{r}})r \\ (m - X_{\dot{u}})u & (-I_z + N_{\dot{r}})r & M_q + M_{q|q|}|q| \end{bmatrix}, \\ \boldsymbol{g}_z = \begin{bmatrix} -(mg - \rho\forall g)\cos(\theta)\cos(\phi) + \ldots \\ (-z_B\rho\forall g)\cos(\theta)\sin(\phi) + \ldots \\ (-z_B\rho\forall g)\sin(\theta) + \ldots \\ \ldots + 0 \\ \ldots + (mw - Z_{\dot{w}}w)v + (I_y + M_q)qr \\ \ldots + (-m + Z_{\dot{w}})uw + (I_x - K_{\dot{p}})pr \end{bmatrix}, \\ \boldsymbol{J}_z(\boldsymbol{\eta}_z) = \begin{bmatrix} \cos(\theta)\cos(\phi) & 0 & 0 \\ 0 & 1 & \sin(\phi)\tan(\theta) \\ 0 & 0 & \cos(\phi) \end{bmatrix}, \\ \boldsymbol{\eta}_z = [z \quad \phi \quad \theta]^T, \quad \boldsymbol{\nu}_z = [w \quad p \quad q]^T \\ \text{and} \\ \boldsymbol{\tau}_z = [Z \quad K \quad M]^T. \end{gathered}$$

In the matrix $\boldsymbol{g}_z$ there are some terms, example: $[(mw - Z_{\dot{w}}w)v]$, which come from the Coriolis matrix and this is related in the velocity variables of the states x, y and ψ, in this part of the control we assuming it like a disturbances.

The first variable of the coordinate change is given by:

$$\boldsymbol{z}_{1z} = \boldsymbol{\eta}_z - \boldsymbol{\eta}_{dz} \tag{20}$$

where $\boldsymbol{\eta}_{dz}$ is the vector desired.

The second variable of the coordinate change is:

$$\begin{aligned} \boldsymbol{z}_{2z} &= \boldsymbol{\nu}_2 - \boldsymbol{\nu}_{vz} \\ \boldsymbol{\nu}_2 &= \boldsymbol{z}_{2z} + \boldsymbol{\nu}_{vz} \end{aligned} \tag{21}$$

where $\boldsymbol{\nu}_{vz}$ (virtual control) is stabilization function of the $\boldsymbol{z}_{1z}$.

Differentiating Equation (20) and combination with Equation (21) and Equation (19)

$$\dot{\boldsymbol{z}}_{1z} = \left[\boldsymbol{J}_z(\boldsymbol{\eta}_z)(z_{2z} + \boldsymbol{\nu}_{vz})\right] - \dot{\boldsymbol{\eta}}_{dz}. \tag{22}$$

The Lyapunov's candidate function is,

$$\boldsymbol{V}_{1z} = \frac{1}{2}\boldsymbol{z}_{1z}^T\boldsymbol{z}_{1z} \tag{23}$$

differentiating the Lyapunov's candidate function and using Equation (22)

$$\dot{\boldsymbol{V}}_{1z} = \boldsymbol{z}_{1z}^T\left(\left[\boldsymbol{J}_z(\boldsymbol{\eta}_z)(z_{2z} + \boldsymbol{\nu}_{vz})\right] - \dot{\boldsymbol{\eta}}_{dz}\right) \tag{24}$$

the virtual control leave the Lyapunov's candidate function to be negative defined, thus

$$\boldsymbol{\nu}_{vz} = -\boldsymbol{J}_z^{-1}(\boldsymbol{\eta}_z)\boldsymbol{K}_F z_{1z} + \boldsymbol{J}_z^{-1}(\boldsymbol{\eta}_z)\dot{\boldsymbol{\eta}}_{dz} \tag{25}$$

with $\boldsymbol{K}_F$ is a positive definite gain matrix. Rewritten Equation (24)

$$\dot{\boldsymbol{V}}_{1z} = -\boldsymbol{z}_{1z}^T\boldsymbol{K}_F\boldsymbol{z}_{1z} + \boldsymbol{z}_{1z}^T\boldsymbol{J}_z(\boldsymbol{\eta}_z)\boldsymbol{z}_{1z} \tag{26}$$

The Lyapunov candidate function for this second step is chosen as

$$\boldsymbol{V}_{2z} = \boldsymbol{V}_{1z} + \frac{1}{2}\boldsymbol{z}_{2z}^T\boldsymbol{z}_{2z} \tag{27}$$

differentiating Equation (27)

$$\begin{gathered} \dot{\boldsymbol{V}}_{2z} = -\boldsymbol{z}_{1z}^T\boldsymbol{K}_F\boldsymbol{z}_{1z} + \boldsymbol{z}_{1z}^T\boldsymbol{J}_z(\boldsymbol{\eta}_z)\boldsymbol{z}_{1z} + \ldots \\ \ldots + \boldsymbol{z}_{2z}^T\boldsymbol{M}_z^{-1}\left[-(\boldsymbol{C}_z(\boldsymbol{\nu}_z) + \boldsymbol{D}_z(\boldsymbol{\nu}_z))\boldsymbol{\nu}_z - \boldsymbol{g}_z(\boldsymbol{\eta}_z)\right] - \ldots \\ \ldots - \boldsymbol{z}_{2z}^T\left[-\boldsymbol{M}_z^{-1}\boldsymbol{\tau}_z + \dot{\boldsymbol{\nu}}_{vz}\right] \end{gathered} \tag{28}$$

Using feedback linearization for the control definition $\boldsymbol{\tau}_z$,

$$\begin{gathered} \boldsymbol{\tau}_z = \boldsymbol{M}_z\boldsymbol{J}_z^T(\boldsymbol{\eta}_z)\boldsymbol{z}_{1z} + [\boldsymbol{C}_z(\boldsymbol{\nu}_z) + \boldsymbol{D}_z(\boldsymbol{\nu}_z)]\boldsymbol{\nu}_z + \ldots \\ \ldots + \boldsymbol{g}_z(\boldsymbol{\eta}_z) + \boldsymbol{M}_z\dot{\boldsymbol{\nu}}_{vz} - \boldsymbol{M}_z\boldsymbol{K}_G\boldsymbol{z}_{2z} \end{gathered} \tag{29}$$

with $\boldsymbol{K}_G$ is a positive definite gain matrix. Replacing Equation (29) into Equation (28)

$$\dot{\boldsymbol{V}}_{2z} = -\boldsymbol{z}_{1z}^T\boldsymbol{K}_F z_{1z} - \boldsymbol{z}_{2z}^T\boldsymbol{K}_G\boldsymbol{z}_{2z} + \boldsymbol{z}_{1z}^T\boldsymbol{J}_z(\boldsymbol{\eta}_z)\boldsymbol{z}_{2z} - \boldsymbol{z}_{2z}^T\boldsymbol{J}_z(\boldsymbol{\eta}_z)\boldsymbol{z}_{1z}. \tag{30}$$

Equation (30) is not negative defined, because of the last two terms $(\boldsymbol{z}_{1z}^T\boldsymbol{J}_z(\boldsymbol{\eta}_z)\boldsymbol{z}_{2z} - \boldsymbol{z}_{2z}^T\boldsymbol{J}_z(\boldsymbol{\eta}_z)\boldsymbol{z}_{1z})$. The presence of the floats become the vehicle stable in ϕ and θ, thus these angles converging easily to zero, consequently, the matrix $\boldsymbol{J}_z(\boldsymbol{\eta}_z)$ becomes diagonal and the last two terms of Equation (30) cancel each other,

$$\dot{\boldsymbol{V}}_{2z} = -\boldsymbol{z}_{1z}^T\boldsymbol{K}_F z_{1z} - \boldsymbol{z}_{2z}^T\boldsymbol{K}_G\boldsymbol{z}_{2z} \tag{31}$$

that way the equation is defined negative.

5. Simulation

For the simulation it was considered the scenario with perturbations in all degrees of freedom of the vehicle, represented by sinusoidal forces/torques. As the basis for the definition of this disturbance was used the same frequency used in the work of Zhu and Gu (2011b),

$$\boldsymbol{\Delta f} = \begin{bmatrix} 22 + 22\sin(0.785t)N \\ 22 + 22\sin(0.785t)N \\ 44 + 44\sin(0.785t)N \\ 10 + 10\sin(0.785t)Nm \\ 11.5 + 11.5\sin(0.785t)Nm \\ 4.5 + 4.5\sin(0.785t)Nm \end{bmatrix} \tag{32}$$

It was used in the simulation of the control two version of HROV: one where the parameters of the plant are correct and other where are considering error in the identification of the parameters and a load with 20% of the original mass. According to Avila (2008) the identification of hydrodynamic parameters is not precise. Thus, analyzing the response of the plant with modeling errors becomes important and a way to show the robustness of the control.

In Table 3 the parameters adopted for the version of the HROV with parameterization error. It was chosen randomly values in a range of thirty percent, more or less (compared to Table 2), of the parameter used

Table 2
Value of the parameters used for the simulation of the controls.

Parameters	Value	Parameters	Value
m	142 kg	K_p	−5 kgm^2/(s.rad)
$m.g$	1391.6 N	M_q	−5 kgm^2/(s.rad)
ρAg	1428.84 N	N_r	−2.27 kgm^2/(s.rad)
z_b	−0.111 m	$X_{u\|u\|}$	−326.6 kg/m
I_x	20.48 kgm^2	$Y_{v\|v\|}$	−1.016.58 kg/m
I_y	19.79 kgm^2	$Z_{w\|w\|}$	−1.706.55 kg/m
I_z	30.83 kgm^2	$K_{p\|p\|}$	−200 kgm^2/rad^2
$X_{\dot{u}}$	−450.5 kg	$M_{q\|q\|}$	−200 kgm^2/rad^2
$Y_{\dot{v}}$	−500 kg	$N_{r\|r\|}$	−111.5 kgm^2/rad
$Z_{\dot{w}}$	−550 kg	$\tau_{(u)}$	−281.44 N → 440.79 N
$K_{\dot{p}}$	−200 kgm^2	$\tau_{(v)}$	0 N
$M_{\dot{q}}$	−200 kgm^2	$\tau_{(w)}$	−562.89 N → 881.59 N
$N_{\dot{r}}$	−162 kgm^2	$\tau_{(p)}$	−190.67 N → 190.67 N
X_u	−41.45 kg/s	$\tau_{(q)}$	−230.39 N → 230.39 N
Y_v	135.0933 kg/s	$\tau_{(r)}$	−95.36 N → 95.36 N
Z_w	311.64 kg/s		

Table 3
Values adopted for the HROV vehicle with parameter identification errors.

Parameters	Value	Parameters	Value
m^*	170.4 kg	K_p^*	−5.5 kgm^2/(s.rad)
$m.g^*$	1669.92 N	M_q^*	−4 kgm^2/(s.rad)
ρAg^*	1709.904 N	N_r^*	−1.59 kgm^2/(s.rad)
z_b	−0.111 m	$X_{u\|u\|}^*$	−391.92 kg/m
I_x^*	20.58 kgm^2	$Y_{v\|v\|}^*$	−813.26 kg/m
I_y^*	17.81 kgm^2	$Z_{w\|w\|}^*$	−1194.59 kg/m
I_z^*	24.66 kgm^2	$K_{p\|p\|}^*$	−160 kgm^2/rad^2
$X_{\dot{u}}^*$	−360.4 kg	$M_{q\|q\|}^*$	−180 kgm^2/rad^2
$Y_{\dot{v}}^*$	−550 kg	$N_{r\|r\|}^*$	−133.8 kgm^2/rad
$Z_{\dot{w}}^*$	−495 kg	$\tau_{(u)}$	−281.44 N → 440.79 N
$K_{\dot{p}}^*$	−240 kgm^2	$\tau_{(v)}$	0 N
$M_{\dot{q}}^*$	−160 kgm^2	$\tau_{(w)}$	−562.89 N → 881.59 N
$N_{\dot{r}}^*$	−194.4 kgm^2	$\tau_{(p)}$	−190.67 N → 190.67 N
X_u^*	−45.60 kg/s	$\tau_{(q)}$	−230.39 N → 230.39 N
Y_v^*	121.58 kg/s	$\tau_{(r)}$	−95.36 N → 95.36 N
Z_w^*	249.31 kg/s		

Table 4
Gains of the controllers.

Controllers gains				
XY Plane	First CLF	$\boldsymbol{K}_a = 5$ $\boldsymbol{K}_b = 5$ $\boldsymbol{K}_c = 1$	$Z\ \theta\ \phi$	$\boldsymbol{K}_F = 50\boldsymbol{I}_{3\times3}$
	Second CLF	$\boldsymbol{K}_D = 100$ $\boldsymbol{K}_E = 100$		$\boldsymbol{K}_G = 100\boldsymbol{I}_{3\times3}$

in the plant control design, except of the vehicle mass.

The parameters of the controllers are show in Table 4.where $\boldsymbol{I}_{3\times3}$ is an identity matrix with size three by three. The desired trajectory chosen for simulation can be seen in Fig. 6.

The error curve of the angle ψ, shown in Fig. 9, appears to present a large error between the simulations with original parameters and with parameter error plus a load of 20% of the original weight. In fact after 50s both errors are almost the same. The only difference is that the system with parameter error performed an extra turn around the *Z* axis and after 50s has stabilized and started the tracking the desired trajectory.

The control effort was required more in the case of the vehicle with parameterization error, as can be observed in Fig. 10, saturating the actuators. This occurs because the initial position of the vehicle is displaced from the trajectory and the vehicle is carrying an unplanned load in the control design.

6. Conclusions

In this paper we design nonlinear multivariable controllers to the tracking problem of the build HROV, as well as it was considered the underactuated model vehicle subjected to nonlinear controllers, unknown disturbances and parameter identification errors with a load of the 28.4 kg.

In all simulations it was considered sinusoidal disturbances acting in all directions. Simulation results verified the efficiency of controllers in the tracking problem.

The proposed controller shows an appropriate performance despite of disturbances as can be observed in Fig. 7 and 8, as well as the controller shows robustness under parameter identification errors.

Designed backstepping controllers guaranteed the global asymptotic stability, their design is simple and the tuning of their parameters is done in a trail-and-error way.

The design of the CLF controller is not a simple task, because the Lyapunov function candidate is not a trivial proposal. The parameter tuning of the CLF controller is more difficult than the backstepping, because the Lyapunov functions candidate is positive semidefinite. This property of Lyapunov function influences in tracking directions to detriment of others directions.

The division of the vehicle model was made in relation to the thrusters, therefore, the horizontally positioned thrusters are responsible for controlling the position of the vehicle in the *XY* plane and turning around the axis *Z*. The others four thrusters is responsible for controlling the position of the vehicle in the *XZ* and *YZ* plane and turning around the axis *X* and *Y*. These division just was used to designed the controllers, which was simulated in the vehicle model without division, like showed in section 3.

The controls showed to be robust because even considering an error in obtaining the parameters and with a load, which represents 20% of the vehicle mass, it was able to perform the tracking of the trajectory.

The backstepping controller has requested a reduced computational cost for its implementation, because the implementation is based in

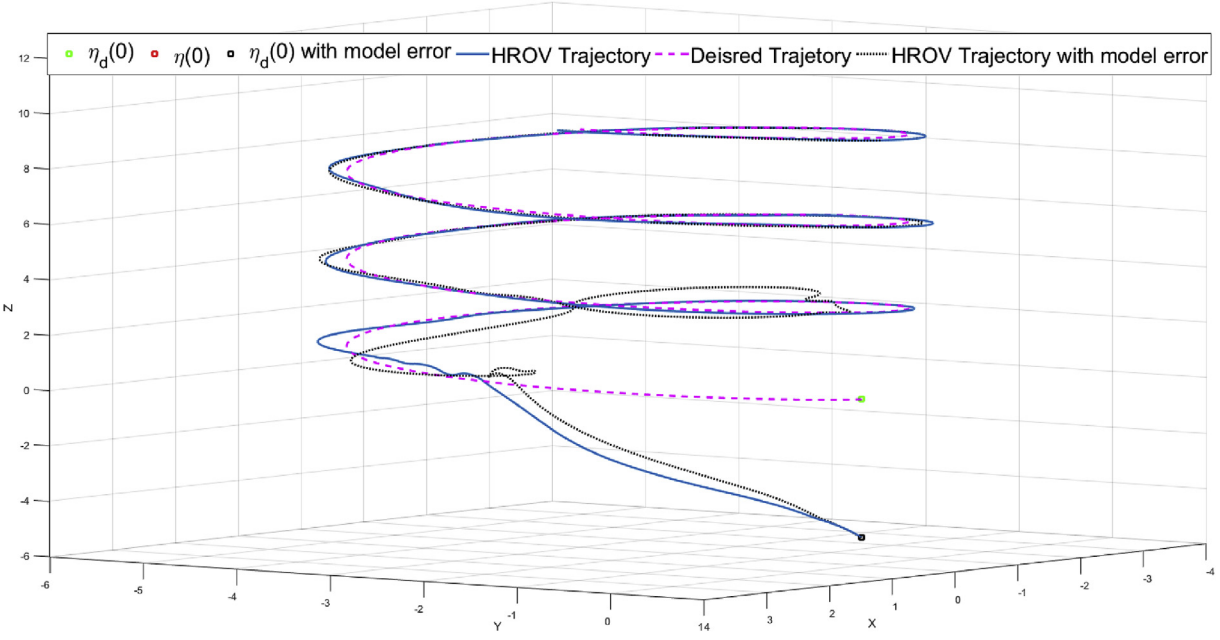

Fig. 6. Trajectory linear simulation results.

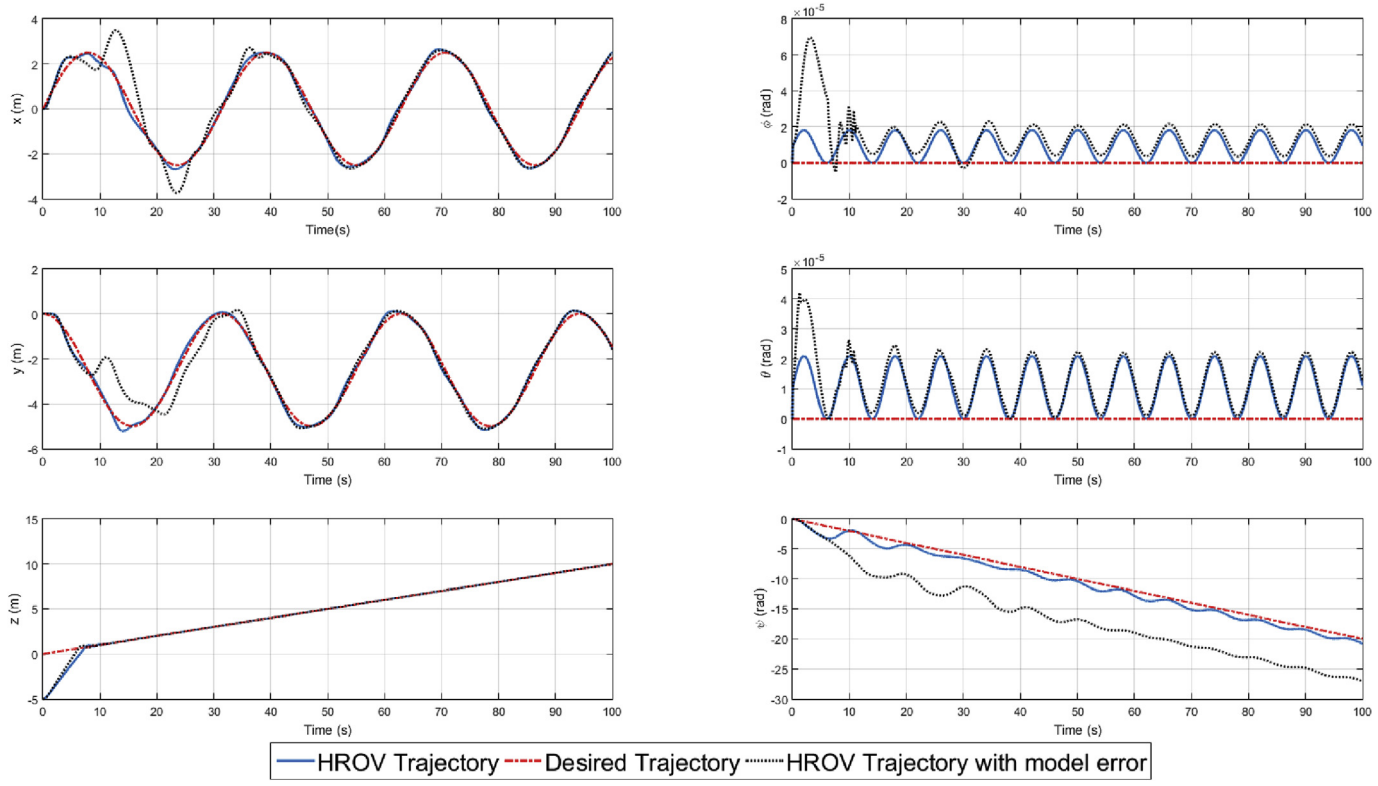

Fig. 7. Trajectory linear and angular simulation results.

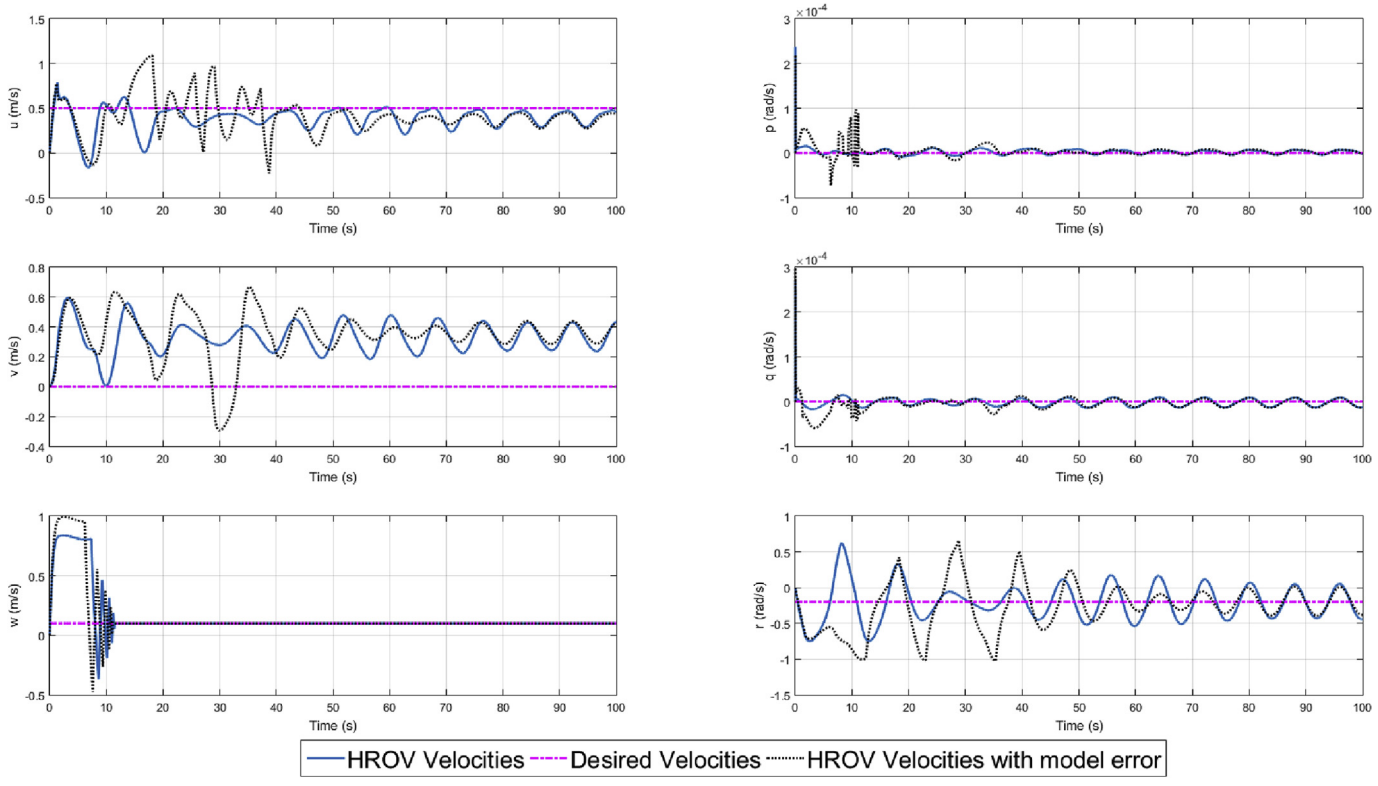

Fig. 8. Velocity linear and angular simulation results.

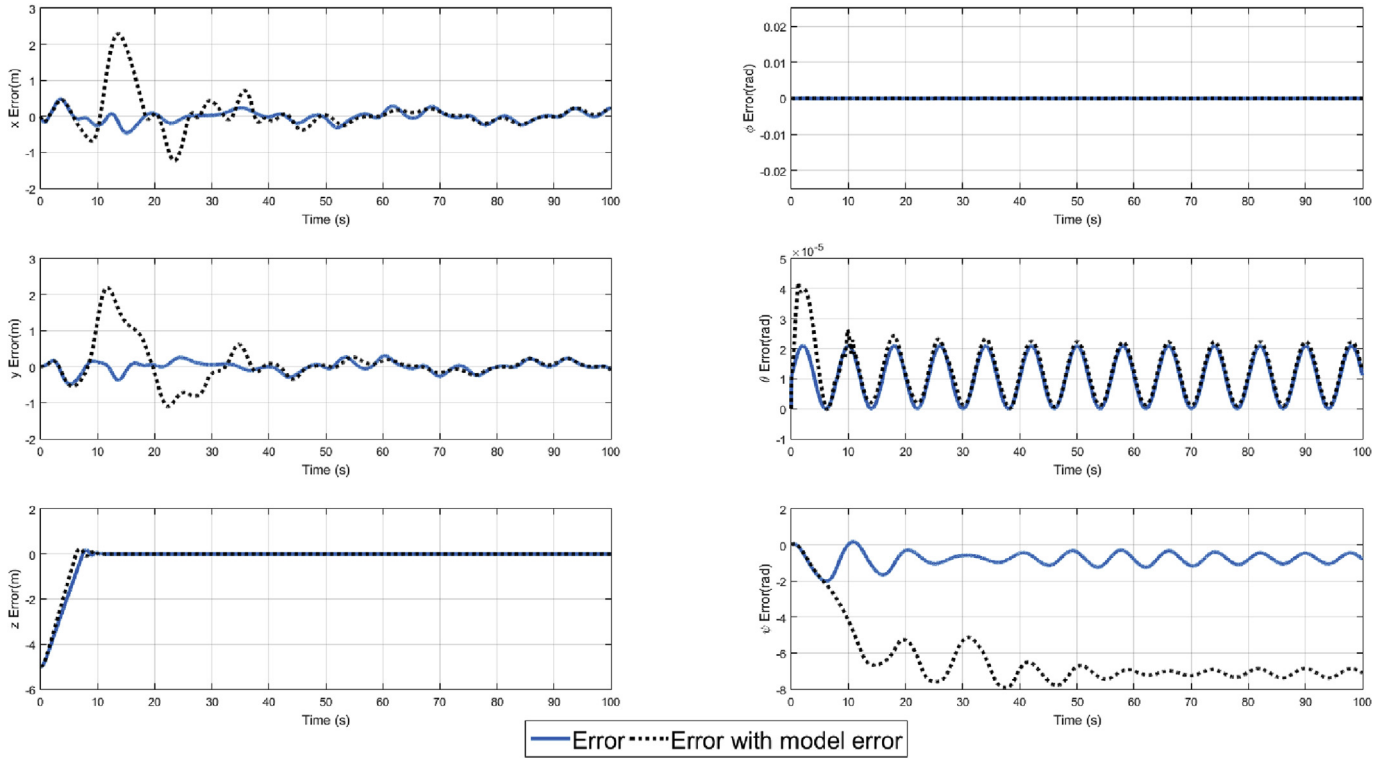

Fig. 9. Trajectory error.

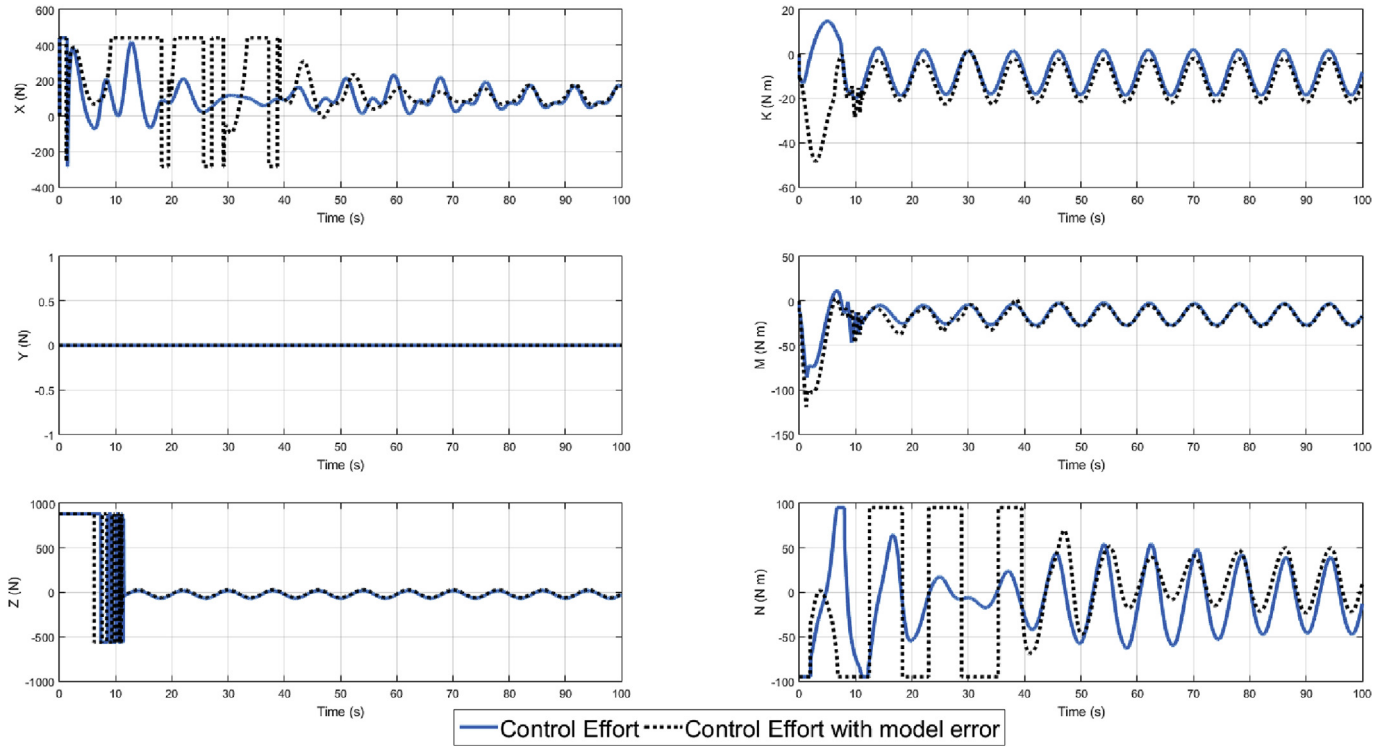

Fig. 10. Control effort.

simple arithmetic operations. Other controller design kinds will be topic of future publication.

References

Avila, J.P.J., 2008. Modeling and Identification of Hydrodynamic Parameters of an Underwater Robotic Vehicle. Doctor of Science in Mechanical Engineering, University of São Paulo in Portuguese. http://www.teses.usp.br/teses/disponiveis/3/3152/tde-03072013-143252/en.php.

Do, K.D., 2010. Practical control of underactuated ships. Ocean Eng. 37 (13), 1111–1119. https://doi.org/10.1016/j.oceaneng.2010.04.007.

Do, K.D., Pan, J., 2009. Control of Ships and Underwater Vehicles: Design for Underactuated and Nonlinear Marine Systems. Springer Science & Business Media.

DPC, 2013. Normas da autoridade marítima para operação de embarcações estrangeiras em águas juridicionais brasileiras. http://www.dpc.mar.mil.br/sites/default/files/normam04.pdf.

Encarnacao, P., Pascoal, A., 2000. 3D path following for autonomous underwater vehicle. In: Decision and Control, 2000. Proceedings of the 39th IEEE Conference on, vol. 3. IEEE, pp. 2977–2982.

Fernandes, D. d. A., Sørensen, A.J., Pettersen, K.Y., Donha, D.C., 2015. Output feedback motion control system for observation class rovs based on a high-gain state observer: theoretical and experimental results. Contr. Eng. Pract. 39, 90–102.

Ferreira, C.Z., Conte, G.Y.C., Avila, J.P.J., Pereira, R.C., Ribeiro, T.M.C., 2013. Underwater robotic vehicle for ship hull inspection: control system architecture. In: COBEM: 22nd International Congress of Mechanical Engineering, vol. 2013, pp. 1231–1241.

Ferreira, C.Z., Conte, G.Y.C., Ribeiro, T.M.C., Avila, J.P.J., 2014. Identification of hydrodynamic parameters for a hybrid rov in a free-flying movement. In: Proceedings of the Twenty-fourth (2014) International Ocean and Polar Engineering Conference, International Society of Offshore and Polar Engineers, Busan, Korea, pp. 363–370.

Ferreira, C.Z., CONTE, G.Y.C., AVILA, J.P.J., RIBEIRO, T.M.C., Pereira, C., 2014. Identification of hydrodynamic parameters for a hybrid ROV in a free-flying movement. In: International Ocean and Polar Engineering Conference (ISOPE), 2014, Busan. Proceedings of the Twenty-fourth (2014) International Ocean and Polar Engineering Conference, pp. 363–370.

Fierro, R., Lewis, F.L., 1995. Control of a nonholonomic mobile robot: backstepping kinematics into dynamics. In: Decision and Control, 1995., Proceedings of the 34th IEEE Conference on, vol. 4. IEEE, pp. 3805–3810.

Fossen, T., 1994. Guidance and Control of Ocean Vehicles. John Wiley & Sons Inc., New York.

Jiang, Z.-P., 2002. Global tracking control of underactuated ships by Lyapunov's direct method. Automatica 38 (2), 301–309.

Khadhraoui, A., Beji, L., Otmane, S., Abichou, A., 2014. Robust control of remotely operated vehicle in the vertical plane. In: Control Automation Robotics & Vision (ICARCV), 2014 13th International Conference on. IEEE, pp. 1098–1105.

LinkQuest Inc., NavQuest 300& 600 Doppler Velocity Log Specifications. URL http://www.link-quest.com/html/NavQuest300600.pdf.

Liu, Z., Wang, N., Zhao, Y., Er, M.J., Li, Z., 2016. Adaptive dynamic surface tracking control of underactuated surface vessels with unknown disturbances. In: Advanced Robotics and Mechatronics (ICARM), International Conference on. IEEE, pp. 382–387.

Luque, J.C.C., Avila, J.P.J., 2013. Surge-yaw control of a hybrid underwater robotic vehicle. In: 22nd International Congress of Mechanical Engineering (COBEM 2013), pp. 7447–7456.

Patompak, P., Nilkhamhang, I., 2012. Adaptive backstepping sliding-mode controller with bound estimation for underwater robotics vehicles. In: Electrical Engineering/Electronics, Computer, Telecommunications and Information Technology (ECTI-CON), 2012 9th International Conference on. IEEE, pp. 1–4.

Raygosa-Barahona, R., Parra-Vega, V., Olguin-Diaz, E., Munoz-Ubando, L., 2011. A model-free backstepping with integral sliding mode control for underactuated ROVs. In: 2011 8th International Conference on Electrical Engineering, Computing Science and Automatic Control, pp. 1–7. https://doi.org/10.1109/ICEEE.2011.6106577. http://ieeexplore.ieee.org/lpdocs/epic03/wrapper.htm?arnumber=6106577.

Srisamosorn, V., Patompak, P., Nilkhamhang, I., 2013. A robust adaptive control algorithm for remotely operated underwater vehicle. In: SICE Annual Conference (SICE), 2013 Proceedings of, IEEE, pp. 655–660.

Tecnadyne A tecnova Inc. Company, Model 1020 DC Brushless Thruster. URL http://www.tecnadyne.com/cms/images/products/pdf/Model%201020%20Brochure.pdf.

Tecnadyne A tecnova Inc. Company, Model 40 DC Brushless Rotary Actuators. URL http://www.tecnadyne.com/cms/images/products/pdf/Model%2040%20Brochure.pdf.

Tritech International Ltd, Altimeter Product Manual: PA200and PA500 Digital Precision Altimeters. URL http://www.tritech.co.uk/media/products/tritech-pa200-pa500.pdf.

Versa Logic Corporation, Reference Manual: Tiger (VL-EPM-24). URL https://versalogic.com/products/manuals/MEPM24.pdf.

Whitcomb, L.L., 2000. Underwater robotics: out of the research laboratory and into the field. In: Robotics and Automation, 2000. Proceedings. ICRA'00. IEEE International Conference on, vol. 1. IEEE, pp. 709–716.

Zhu, K., Gu, L., 2011. A MIMO nonlinear robust controller for work-class ROVs positioning and trajectory tracking control. In: 2011 Chinese Control and Decision Conference (CCDC). IEEE, pp. 2565–2570.

Zhu, K., Gu, L., 2011. A mimo nonlinear robust controller for work-class rovs positioning and trajectory tracking control. In: 2011 Chinese Control and Decision Conference (CCDC). IEEE, pp. 2565–2570.

Zhu, K., Gu, L., Chen, Y., Li, W., 2012. High speed on/off valve control hydraulic propeller. Chin. J. Mech. Eng. 25 (3), 463–473. https://doi.org/10.3901/CJME.2012.03.463. https://doi.org/10.3901/CJME.2012.03.463.

Zidani, G., Drid, S., Chrifi-Alaoui, L., Benmakhlouf, A., Chaouch, S., 2015. Backstepping controller for a wheeled mobile robot. In: 2015 4th International Conference on Systems and Control (ICSC). IEEE, pp. 443–448.